HELICOPTER ENGINE PERFORMANCE SIMULATIONS ACCOUNTING FOR INTAKE DISTORTIONS

F. Fuchs, V. Gümmer
Lehrstuhl für Turbomaschinen und Flugantriebe, Technische Universität München

Abstract
Subject of this work is the investigation of the impact of inlet distortions on helicopter gas turbines. These small turboshaft engines encounter a wide field of inhomogeneous inlet flows as a result of their specialized usage. By using the *Matlab/Simulink*® tool-box *Toolbox for the Modeling and Analysis of Thermodynamic Systems* (T-MATS) a performance calculation tool is implemented to predict the impact of a distortion to the engines thermodynamic cycle. In its first version, presented in this paper, it is able to address total pressure distortions, but the approach taken will also be able to treat temperature distortions later on. To confirm the calculated results a series of tests were executed on a helicopter engine test bed, which includes a common small turboshaft engine for around 300-600kW shaft power used in light twin-engine helicopters.

1. ABBREVIATIONS AND INDIZES

T-MATS	Toolbox for Modeling and Analysis of Thermodynamic Systems
MTOW	Maximum Take-Off Weight
AIP	Aerodynamic Interface Plane
NASA	National Aeronautics and Space Administration
ISA	International Standard Atmosphere
$DC60$	common distortion describtor
$_{dis.}$	abbreviated for distortion
MGT	Measured Gas Temperature – used as characteristic temperature for engine cycle
N_g	speed of the gas generator
$_{norm}$	data normalized to ISA-conditions
Θ	angle of the distortion size
$\bar{p}$	averaged pressure
P_{shaft}	engine output shaft power
$R\text{-}line$	auxiliary coordinate to describe an explicit point in the performance map

2. INTRODUCTION

Due to the lack of alternative propulsion concepts and their advantageous power-to-weight-ratio for an output power of around 250 kW and larger [18], small turboshaft engines are nearly the unique power source for helicopters with above 2 to MTOW. To realize a compact layout of the whole propulsion system in small helicopters, the engines are mostly mounted in the upper part of the fuselage, next to the main gearbox and the rotor, as shown in Figure 1.

Figure 1: H135, typical small twin-engine helicopter with integrated engine design. Engine position marked with a red circle. Picture based on [1].

This type of engine integration leads to complex air inflow ducts, which cause the inlet flow field to deviate from an ideal homogeneous flow profile at the compressors face, often called *Aerodynamic Interface Plane* (AIP). A comprehensive wind tunnel investigation of intake duct layouts, exemplarily for a H135 related helicopter, was presented in [12]. The results clearly show a non-uniform total pressure profile at the AIP. To be able to predict the performance influences of such distortions during the design phase of a helicopter, a performance simulation tool was implemented by using the Matlab/Simulink® software package. To represent the turbomachinery components a tool box developed by *NASA* at the *Glenn Research Center* called T-MATS is used [6]. It also provides the numeric Newton/Raphson-solver to calculate the state of the engine model. To verify the model, its behavior is checked for plausibility of the results and it is compared to a series of engine tests carried out on a common small turboshaft engine. The test bench engine is used for delivering the fundamental performance data for the T-MATS model, as well.

doi:10.25967/530046

3. THE ENGINE MODEL

As mentioned, a modern small turboshaft engine with a range of around 300 to 500 kW maximum continuous shaft power is the basis for the numeric engine model. The engine has a two-shaft design, which is in common with other competitors. The gas generator shaft connects the single-stage centrifugal compressor and the single-stage axial high-pressure turbine. The power shaft connects the single-stage axial low pressure (power turbine) via a gearbox with the helicopters drive chain. Shortly describing the engines basic function in a few words, the gas generator, working according to a simple Joule-Brayton gas turbine cycle, provides the hot and pressurized gas stream used in the free-turning power turbine, which in turn supplies the desired output shaft speed and torque. As the entire main rotor system in helicopters is designed to a fix rotational speed, a change of the load directly translates to a change of the power turbines torque. The engine can vary its power output by changing the amount of fuel burnt in the combustor, which results in a higher speed of the gas generator shaft and in a larger and higher pressurized exhaust mass flow in front of the power turbine. The engines gearbox reduces the power turbine speed to the much lower speed of the engines drive shaft.

3.1. Implementation in T-MATS

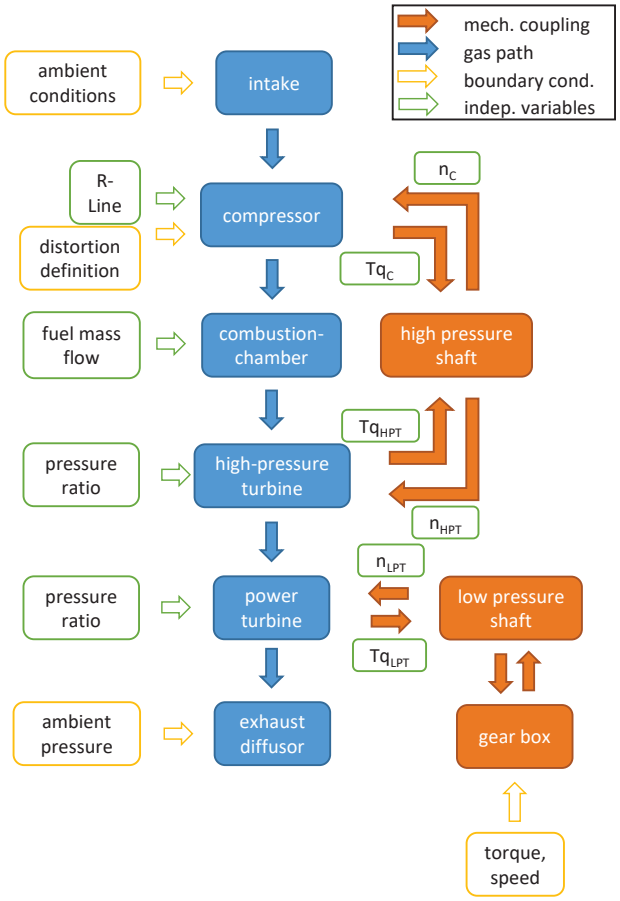

Figure 2: Schematic setup of the engines T-MATS model.

To build up the engine model the T-MATS tool-box provides blocks for each component in a gas turbine cycle. Along the gas path the blocks hand over the local fluid characteristics, like e.g. total temperature T_t, total pressure p_t and the total enthalpy h_t. The mechanical connection between the turbo components and the shafts is realized by the speed n and torque Tq data including loss coefficients. A schematic overview is given in Figure 2. With the boundary conditions of the model, marked in yellow, the solver iterates the independent variables, marked in green to solve the equation system. The mass flow differences over one block and the time derivative of the rotational speeds are used as dependent variables and should become approximate zero during the solution process for a stationary operating point.

3.1.1. Turbo Components and Scaling

In the engine cycle simulation, the turbo components performance is usually described by their maps of pressure ratio, mass flow and efficiency. As the lines of constant reduced speed n_{red} in compressor maps normally have a vertical segment, which results in different pressure ratios π for the same speed setting, a special *R-Line* is used in T-MATS. This *R-Line* is an increasing value along one speed line starting at the surge line with the value 1 and ending at the choke line with 3. This removes the ambiguity and each point can be clearly addressed by a speed line n_{red} and a *R-line* value. For the turbine maps the reduced speed line n_{red} and the pressure ratio π is used to describe each single point, since there is no danger of ambiguity for some values [7]. As the original performance maps of the underlying engine turbo components are unpublished, representative maps have been generated. For the compressor a performance map from a research centrifugal compressor, published in the early 90s is used [3]. Its dimensions are around 40-50% larger than the true engine compressor, but based on the year it should be around the same technology level. The map parameters were taken from [15] and scaled accordingly to [13] using a predicted design point of the engines compressor. The turbines are represented by available maps at the institute for a different helicopter engine with just slightly less performance range. These were scaled according to [13] as well. Nevertheless, to achieve a precise matching between real engine and the simulated engine it could be necessary to not just scale the maps for the design point but also match the off-design range [5]. T-MATS provides the iDesign function to address this need. This leads to a field of variable scaling factors for the maps where, depending on the power setting, the most suitable scaling factors are interpolated. In this case, engine deck data from the test engine was used as benchmark for this scaling.

3.1.2. The Parallel Compressor Model

To consider a distorted inflow in performance calculations of an engine the parallel compressor method is state of the art. It was first introduced by [16] in the late 50s and since then refined by including considerations about a minimum distortion size to affect a compressor at all [17]. A detailed consideration of this minimum distortion size Θ_{crit} is given in [8].

Basically, the parallel compressor model is based on the assumption that a compressor with a partial distorted inflow can be divided into two individual compressors working in parallel and being simulated separately. Each of the two compressors will have an individual inflow condition, depending on the inflow distortion description, and will take

a fraction of the overall mass flow depending on the distorted area at the compressor inlet face.

$$\dot{m}_{red,segment} = \frac{\theta}{360°} \cdot \dot{m}_{red,total} \quad (1)$$

Finally, the parallel compressors feed a common backside what results in an equal back-pressure for the both of them. Figure 3 shows the sketch of a single distortion parallel compressor model with a distortion sector size Θ, colored in red. In case of more than one distorted segment, the model is extended by additional parallel compressors.

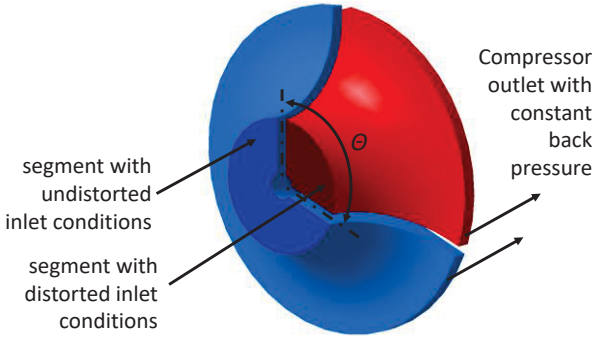

Figure 3: Sketch of a parallel compressor model with a distortion size of Θ.

When considering a one-per-rev total pressure distortion, comparable to the configuration in Figure 3, a new operating point can be estimated with the following method: For both parallel compressors a new operating point is calculated, obviously under consideration of a scaled reduced mass flow $\dot{m}_{red}$ abscissa, depending on the distortions extension and the different inlet conditions inside and outside of the distortion. As the reduced speed n_{red} is not affected by the inlet pressure, both compressors must stay on the same speed line. The operating point of the distorted segment will be shifted towards higher pressure ratios, since it must compensate the lower local inlet pressure. Finally, the new operating point of the whole compressor is averaged by using a mass flow balancing from the separate operating points of the parallel compressors. In case the operating point of the distorted segment reaches the compressors stability limit, the whole compressor will become unstable. A graphic description is displayed in Figure 4.

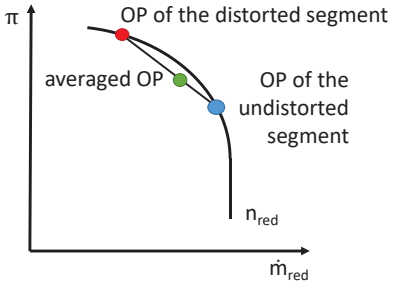

Figure 4: Description of the different operating points (OP) for the parallel compressors in a compressor map.

This method is implemented in T-MATS by replacing the standard compressor block by a separate sub-function. The sub-function is a rebuild of multiple parallel compressors, which are fed by a splitter block, that separates the mass flow according to the distortion definition. Depending on the distortion, respectively a set of inlet conditions and an abscissa scaled compressor map is passed to each compressor. At the compressors backend a mixing block averages the different outflows and guaranties the required common outlet conditions. The total torque to drive the compressor is summed up over all parallel compressor torques.

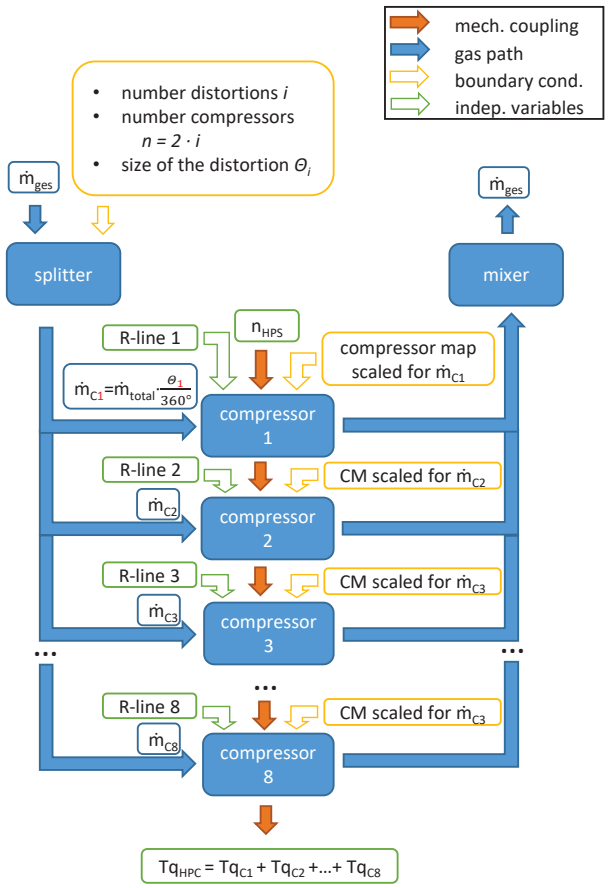

Figure 5: Schematic display of the parallel compressor model implementation (in the compressor block of Figure 2)

Depending on the number of distorted sections x_{dis} a controlling enables the necessary number of parallel compressors x_{comp}.

$$x_{comp} = 2 \cdot x_{dis} \quad (2)$$

The model is implemented for a maximum of eight parallel compressors, which results in a maximum of four distorted sections. This limit was chosen, because an increasing number of single distortions reduces their geometrical extension, resulting in a massive declining impact to the compressors performance of each particular distortion. Remember the relevance of the minimum distortion size Θ_{crit} above. Due to the limitation of the solver to only handle a fixed number of input variables an adaption needs to be introduced: provide and activate an individual solver for all potential parallel compressor configurations, which offers the exact fitting configuration of input and boundary variables.

4. THE MODLES BEHAVIOUR

Since the model is based on data of an engine, several fundamental performance values for a varying power setting are compared between three sets of data: the T-MATS model, the engine deck (a performance model provided by the engine manufacturer), and values from engine testing. The delivered shaft power P_{shaft} is normalized using an unpublished reference value due to disclosure restrictions.

Figure 6 shows the Measured Gas Temperature *MGT*, a measured turbine outlet temperature corrected with ambient temperature and shaft speed referred factors, described in the engines installation manual. A good conformity between engine deck and T-MATS model is given. However, a distinctive difference between the tested and the simulated engines of up to 10% for low power settings can be observed. It noticeably improves towards high performance points, reducing down to about 2%. This discrepancy also occurs between the institute's engine test data and test data of the engine manufacturer. Since the test procedure of the manufacturer is not disclosed and unknown, the error is suspected to be somewhere in the method of testing and measuring the *MGT* at the institute's engine test bed.

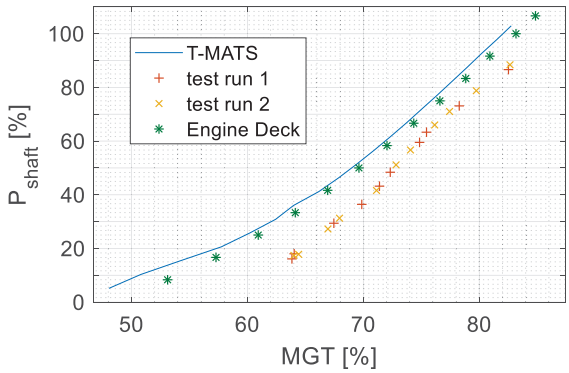

Figure 6: MGT for different power settings for simulated and real engine

When considering the gas generator speed N_g in Figure 7 a good agreement of the data can be observed. Just a slight offset of less than 1% for higher power settings between the T-MATS model, the tested engine and the connected engine deck is detectable. That is considered a relatively good agreement.

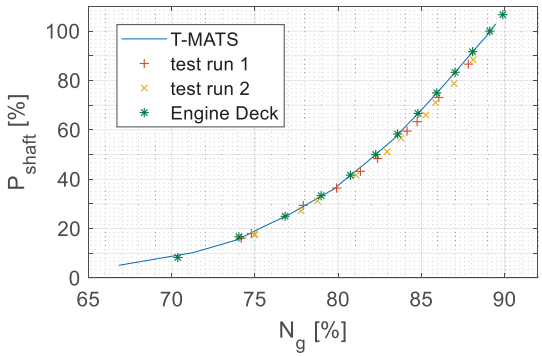

Figure 7: N_g for different power settings for simulated and real engine

The same can be stated for the compressors pressure ratio π in Figure 8. The discrepancies between the T-MATS model, the engine deck and the tested engine is always equal or less than about 2%. This deviation is increasing towards its maximum of around 2% for the highest output power.

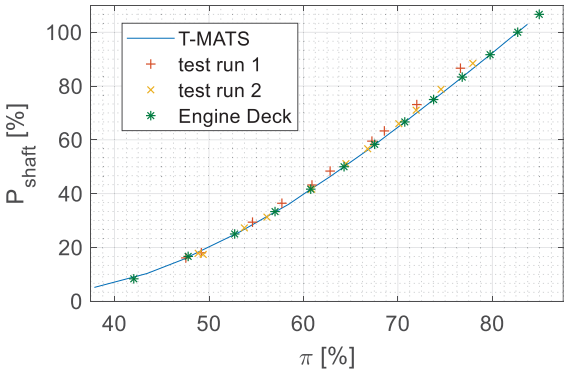

Figure 8: π for different power settings for simulated and real engine

In a second step, after evaluating the T-MATS models basic engine cycle, a closer look should be given to the parallel compressor and its simulation behavior. First a review of the distortion itself is done. It can be described with several different indices [9]. In the European turbomachinery community the distortion parameter *DC60* (3) is widely used [4]. It compares the mean pressure of the most distorted 60°-segment $\bar{p}_{t,60°}$ with the averaged total pressure $\bar{p}_{t,AIP}$ in the whole AIP [14], non-dimensionalised using dynamic head.

$$DC60 = \frac{\bar{p}_{t,AIP} - \bar{p}_{t,60°}}{\rho/_2 \cdot \bar{v}^2} \tag{3}$$

Implemented in T-MATS, each total pressure distortion, indexed with *i*, is directly described by its pressure ratio between the corresponding distorted and the undistorted segment(s) (4).

$$\pi_{dis} = \frac{\bar{p}_{t,distorted,i}}{\bar{p}_{t,undistorted}} \tag{4}$$

This has the advantage of the ability to transfer pressures directly, without conversion, to the model.

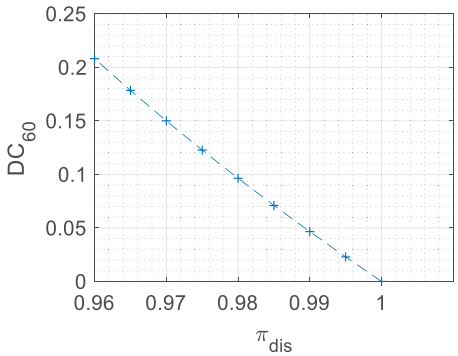

Figure 9: Connection between DC60 and π_{dis}.

The relation between these two possible distortion descriptions is given in Figure 9. It shows the correlation for a fixed 60° distorted segment with a changing total pressure loss within this segment.

The pressure ratio π for both parallel compressors is changing along the distortions intensity, as shown in Figure 10. With an increasing intensity the inlet pressure to the distorted compressor is decreasing, which in contrast to this leads to a higher pressure ratio π. The slight increase in overall pressure ratio for an increasing distortion can be explained by the following consideration. A distorted inflow also decreases the engines mass flow to some extent. As the model is implemented with the delivered output power as a boundary condition it compensates a lack in mass flow with a little increase in total pressure ratio for the averaged compressor to ensure the necessary enthalpy difference in the power turbine.

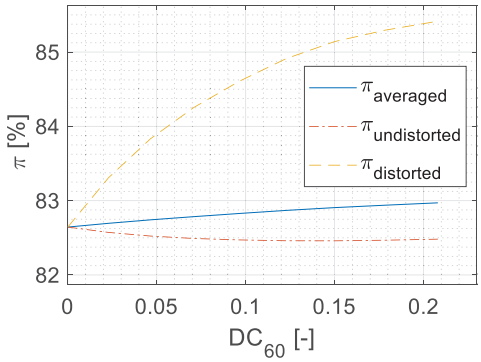

Figure 10: The parallel compressors pressure ratio π for a single distortion with increasing distortion intensity

For more than one distorted segment, the different operating points in Figure 11 for each parallel compressor are defined according to the above mentioned theory. The two distortions shown are of the same size but with different intensities. Depending on their intensity, the operating point moves closer towards the surge line (marked in red). The red dot indicates the new averaged operating point used for the full engine cycle calculation.

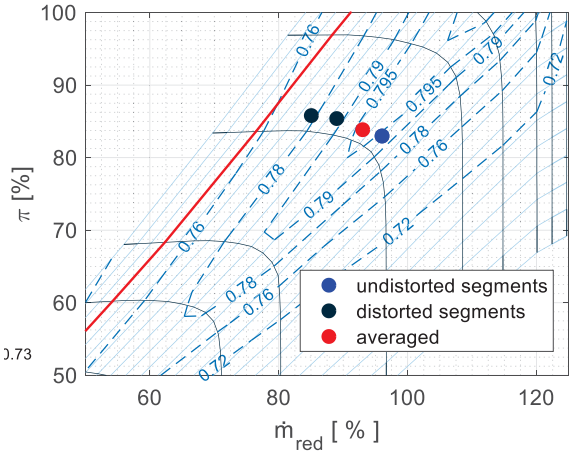

Figure 11: operating points for distorted and undistorted segments and the new average in a partial compressor map with the surge line in red.

A distortion affects not only the compressor, but may also visibly change the engine cycle. To show the impact on the cycle the specific fuel consumption *SFC* is chosen, as it directly represents the cycles efficiency. As displayed in Figure 12 it affects the *SFC* in a negative way. When the distortion intensity increases, the *SFC* percentage is rising as well - representing a degradation of the overall engine efficiency.

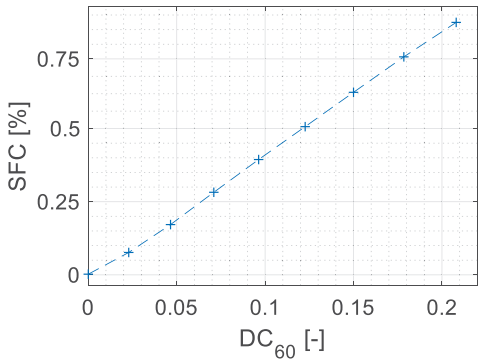

Figure 12: The T-MATS engines specific fuel consumption increase for a fixed power setting with increasing distortion intensity.

Since the mixing block is averaging the gas path parameters at the parallel compressors back end, the overall efficiency can not be read out from the drawn compressors map anymore. The new total operating points efficiency is always shifted to a lower level than the original efficiency distribution in the map [17]. This leads to greater compressor work, which must be thermodynamically compensated by the cycle process. Therefore, less output power is available for the same fuel mass flow, what is represented by the SFC.

5. COMPARISON WITH ENGINE TEST DATA

Finally, the results of the engine cycle simulation shall be compared to engine test data. In order to enable this, on the test bed special pressure screens have been used at the entry of the engine intake to expose the engine to total pressure distortions of varying size and intensity.

To generate the distortions, perforated alloy sheets where mounted in the inlet plenum of the engine. The plenum normally ensures an equal air distribution around the full radial engine inlet. For changing the intensity the screens were repeatedly manufactured with the same drilling pattern, but with different hole diameters and further, for some tests, were partly or fully covered for highest intensity. The inlet plenum with and without mounted distortion generator is shown in Figure 13.

The compared distortions simulated with T-MATS are provided with a dynamic component, since the tested perforated sheet distortions have a drag depending on the flow velocity. The flow velocity in the inlet changes linearly with the air mass flow through the engine. This in turn is determined by the engines power output. As a result, the simulated distortions must be stronger for high engine loads than for low loads. A rough estimation of the distortion intensity was carried out on a wind tunnel model of the inlet using the measurements presented in [11]. This procedure is necessary because there is no way to fully measure the distortion in the AIP on the engine itself.

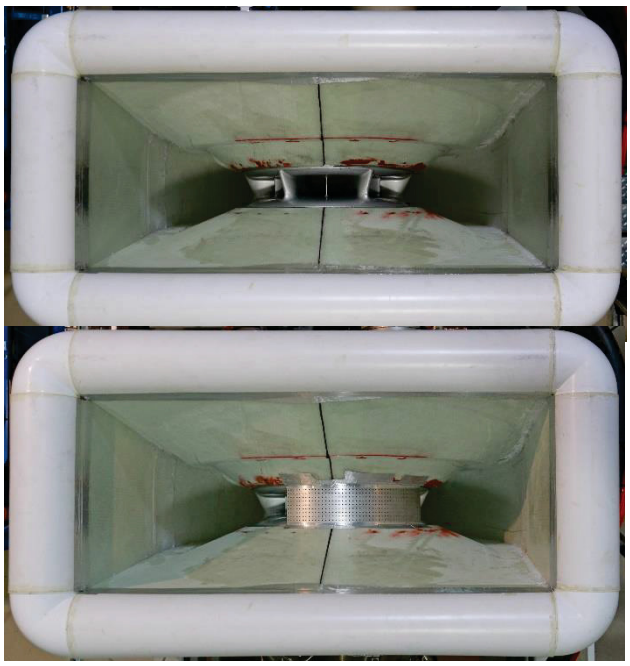

Figure 13: Inlet plenum with engine intake in the upper picture and mounted distortion generator for a 90° distortion in the lower picture

To determine the engines reaction to intake distortions, stationary operating points where recorded over a wide field of the engines performance. These performance points are distributed over the full test facility range with 5%-steps in engine torque and maintained for at least over a minute, whereas the last ten seconds where used for averaging the stationary data. This is necessary to eliminate thermal adaption processes within the engine when changing the power and consecutively temperature levels [10]. To determine an operating line for each distortion configuration a polynomial, which is originally best fitting to engine deck data, is shifted along the abscissa (x-direction). This shift is done such, that the lowest squared distances to all connected measured data points is reached.

$$min\left[\sum_{n=1}^{k}\left(X_{OP,k}-X_{ED,k}\right)^2\right] \tag{5}$$

With k being the number of measured data points, $X_{OP,k}$ the x-value of each point and $X_{ED,k}$ the x-value for the same P_{shaft} from the engine deck.

Figure 14 shows the normalized MGT_{norm} towards different normalized power settings $P_{shaft,norm}$ for a varying distortion size of equal intensity. The semicolon-line represents the T-MATS model data and the continuous lines represent the measured operating lines, obtained by the shift of an engine deck line described above (5). Normalization of the test data is done according to [19] by using ISA-conditions. The T-MATS model is directly calculated for ISA-conditions. The given reference lines are for a non-distorted engine intake. Comparing both sets of data, the T-MATS and the real engine, a similar impact, pictured by the lines diversification, of the distortion towards the engines *MGT* is detectable. Anyway, the total discrepancy between the T-MATS model and the real engine at the *MGT* still exists.

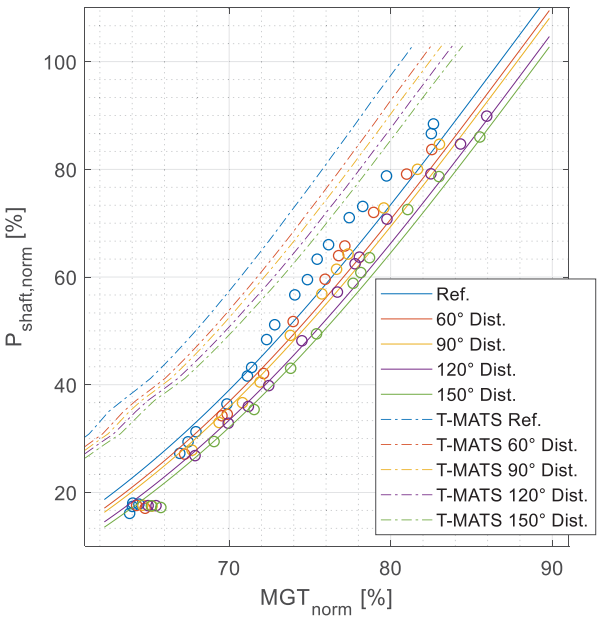

Figure 14: Comparison of MGT operating lines for T-MATS-model and the engine deck operating lines shifted according to (5) using the measured points, shown as colored dots.

In the next Figure 15, basically the same content is shown, but for the normalized gas generator speed $N_{g,norm}$ on the abscissa, instead of the *MGT*. The semicolon-lines are describing the T-MATS data, again.

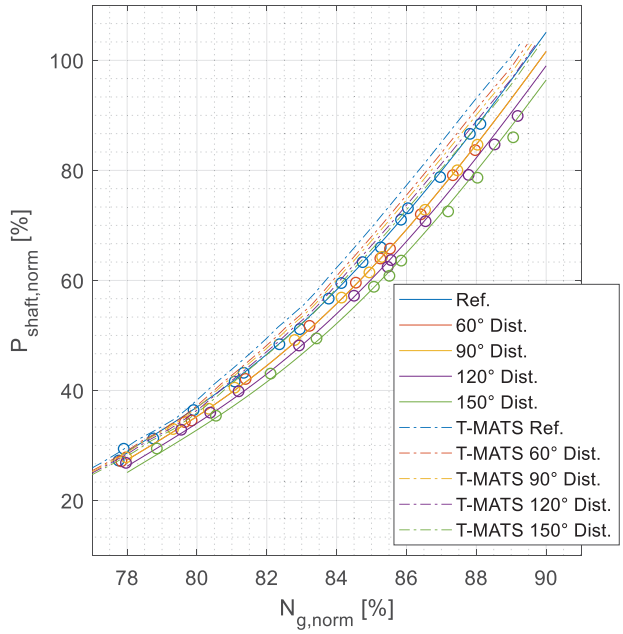

Figure 15: Comparison of N_g operating lines for T-MATS-model and the engine deck operating lines shifted according to (5) using the measured points, shown as colored dots.

Equal to the prior figure the continuous lines, show the shifted engine deck operating line to fit the measured data, displayed with the dots. The impact of the distortions towards the operating lines of the T-MATS model and the test engine seems to be comparable. Apparently, a distortion affects the T-MATS cycle in a similar way as the real engines cycle.

To review the engines compressor behavior a look to the reached pressure ratio for a given compressor speed is shown in Figure 16.

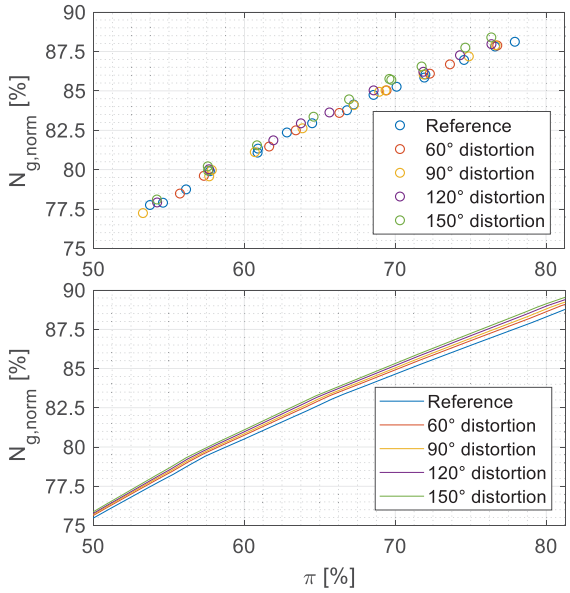

Figure 16: Impact to the compressor pressure ratio π for a varying distortion size at the tested engine (upper figure) and for the T-MATS model (lower figure).

For an increasing distortion size *Θ*, displayed with different colors, the reached pressure ratio *π* for a given compressor speed $N_{g,norm}$ is reducing. This can be stated for the tested engine in the upper figure and for the T-MATS model in lower figure as well. The quantitative impact seems to be comparable between both sets of data, with less than 1% impact on low power settings and up to 2-3% for a high-power setting with high pressure ratios and a large gas generator speeds. This behavior corresponds to the expected effect that a distortion has a negative effect on the reachable pressure ratio π of the compressor. Especially for a centrifugal compressor, as the engine is equipped with a single stage centrifugal compressor, this behavior is shown in [2]. In the mentioned publication, a centrifugal compressor is tested on a component test bed to neglect the influences provoked from other engine parts.

6. CONCLUSION

The T-MATS model with an implemented parallel compressor model leads to predictable results for the compressor, but also for the whole engine cycle. When looking on overall performance characteristics it shows the estimated behavior in case of a pressure distortion occurs. The thermodynamic cycle is stressed by an increasing distortion, what is figured for the measured gas turbine *MGT* and the gas generator speed N_g. Finally, the overall efficiency, represented with the *SFC,* is decreasing. The compressors operation is directly affected by the distortion, it demonstrates the predicted shift towards a degraded performance.
To verify the distortions impact to the engine cycle a series of engine tests for different total pressure distortion configurations was executed and compared to the T-MATS model data. A good accordance was displayed.
Another drawback is, that as long as the model is based on turbo component performance maps, which are not the original ones from the based engine, the exact position of the compressors stability limits is unknown. A prediction of a critical distortion, that leads to engine instabilities, is not accurate in this case, since it just shows the loss of stability for the used deviant modeled compressor.
In summary, this means that with the presented T-MATS model a first loss of performance prediction is feasible to evaluate the engine mounting and integration situation. This could help to reduce the financial and operational risks, when designing a new helicopter engine intake. However, always a critical view must be taken to the danger of stability failures, at least without the compressor manufacturers original performance map.
In a next step the model should be expanded to give the possibility of considering temperature distortions. They have a high relevance for helicopter engines as well [20]. Exemplary the hot exhaust flow of the engine can be easily transported by the turbulent rotor downwash towards the engine intake. The parallel compressor model directly can be applied for these considerations, but the controlling of inlet and boundary conditions must be adapted. Since temperature distortions often have a very dynamic occurrence, the model could made use of the T-MATS given possibility of executing dynamic engine simulations.

7. ACKNOWLEDGMENTS

The research presented in this paper has been strongly supported by two master students, who wrote their thesis at the institute: Mr. P. Maas and Mr. V. Brandtner considerably contributed to development process of the *T-MATS* model. Many thanks to them for their great contribution to the development process of the basic engine model and the parallel compressor method implementation.
Further the whole project has been partially funded in the scope of the CHARME research project by the German Federal Ministry of Economics and Energy (FKZ 20H1501A) and has received great support from the project partner Airbus Helicopters Deutschland.

8. REFERENCES

[1] Airbus Helicopters. *Paint Scheme Configurator*. http://www.airbushelicopters.com/paint/index.htm. Accessed 20 November 2019.

[2] Ariga, I., Kasai, N., Masuda, S., Watanabe, Y., and Watanabe, I. The Effect of Inlet Distortion on the Performance Characteristics of a Centrifugal Compressor. In *Journal for Engineering and Power*, 223–230.

[3] Belaygue, P. and Vignau, H. 1993. Le compresseur centrifuge, composant essentiel des turbomoteurs de petite et moyenne puissance. In *Technology Requirements for small Gas Turbines*. *AGARD Conference Proceedings No. 537*.

[4] Bissinger, N. C. and Breuer, T. Basic Principles – Gas Turbine Compatibility – Intake Aerodynamic Aspects. In *Encyclopedia of Aerospace Engineering*.

[5] Chapmann, J. W., Lavelle, T. M., and Litt, J. S. 2016. *Practical Techniques for Modeling Gas Turbine Engine Performance* NASA/TM-2016-219147. Glenn Research Center; Vantage Partners.

[6] Chapmann, J. W., Lavelle, T. M., May, R. D., Litt, J. S., and Guo, T.-H. 2014. *Toolbox for the Modeling and Analysing of Thermodynamic Systems*. *T-MATS*. MATLAB/SImulink Tool-Box. National Aeronautics and Space Administration, Glenn Research Center.

[7] Chapmann, J. W., Lavelle, T. M., May, R. D., Litt, J. S., and Guo, T.-H. 2014. *Toolbox for the Modeling and Analysis of Thermodynamic Systems (T-MATS) - User's Guide* NASA/TM-2014-216638. Glenn Research Center, Vantage Partners.

[8] Cousins, W. T. 1998. *A Theory for the Prediction of Compressor Blade Aerodynamic Response* AIAA-98-3308. 34th Joint Propulsion Conference, Cleveland.

[9] Cousins, W. T. 2004. *History, Philosophy, Physics and future Directions of Aircraft Propulsion System/ Inlet Integration* GT2004-54210. Pratt & Whitney, ASME Turbo Expo, Vienna.

[10] Deutsches Institut für Normung. 1979. *Abnahmeregeln für Gasturbinen*. Beuth Verlag GmbH, Berlin, DIN 4341-1.

[11] Fuchs, F., Schäffer, C., and Gümmer, V. 2018. *Experimental Investigation of a Radial Turboshaft Engine Intake* 10.2514/6.2018-4747. AIAA Propulsion and Energy Forum - Joint Propulsion Confernece, Cincinnati, Ohio.

[12] Knoth, F. and Breitsamter, C. 2017. Aerodynamic Testing of Helicopter Side Intake Retrofit Modifications. *MDPI - Aerospace* 2017, 4 (Jun. 2017).

[13] Kurzke, J. 1996. *How to get Component Maps for Aircraft Gas Turbine Performance Calculations*. MTU Aero Engines, International Gas Turbine and Aeroengine Congress & Exhibition, Birmingham, UK.

[14] Kurzke, J. 2006. *Effects of Inlet Flow Distortion on the Performance of Aircraft Gas Turbines* GT2006-90419. Gas Turbine Performance Simulation Software, ASME Turbo Expo, Barcelona.

[15] Kurzke, J. and GasTurb GmbH. 2017. *GasTurb*. GasTurb GmbH, Aachen, Deutschland.

[16] Pearson, H., McKenzie, A. B. 1959. Wakes in Axial Compressors. In *Journal of the Royal Aeronautical Society*, London, 415–416.

[17] Reid, C. 1969. *The Response of Axial Flow Compressors to Intake Flow Distortion*. Rolls-Royce Limited, Aero Engine Divison, ASME Gas Turbine Conference & Product Show, Cleveland.

[18] Rick, H. 2013. *Gasturbinen und Flugantriebe*. Springer, Berlin, Heidelberg.

[19] SAE Aerospace. 2013. *Turboshaft/Turboprop Gas Turbine Engine Test Cell Correlation*. SAE International, ARP4755.

[20] Turczeniuk, B. 1979. *Exhaust Gas Reingestion Measurements*, AHS Southeast Region Propulsion Specialist's Meeting, Williamsburg, VA.